SLAC-PUB-1666
November 1975
(T/E)

HADRON PRODUCTION AT SPEAR*

R. F. Schwitters

Stanford Linear Accelerator Center
Stanford University, Stanford, California 94305

* Work supported by the U.S. Energy Research and Development Administration.
(Invited paper presented at the International Symposium on Lepton and Photon Interactions, Stanford University, Stanford, California, August 21-27, 1975.)

HADRON PRODUCTION AT SPEAR*

R. F. Schwitters

Stanford Linear Accelerator Center
Stanford University, Stanford, California, USA

I. INTRODUCTION

The first measurements of hadron production at the SPEAR electron-positron storage ring began at the time this Symposium last met in Bonn just two years ago. At that conference[1] our knowledge of hadron production in e^+e^- interactions could be summarized by the graph in Fig. 1, where the quantity R, the ratio of the total cross section for producing hadrons σ_T, to that for producing muon pairs is plotted versus s, the square of the center-of-mass (c.m.) energy. The pioneering work done at the Frascati,[2] Orsay,[3] and Novosibirsk[4] laboratories had shown that hadrons are produced with relatively large cross sections in e^+e^- interactions, comparable to mu-pair production. Then, at Bonn, the spectacular results from CEA[5] were available and R was seen to step boldly through the popular theories of the day.

The first results on the total hadronic cross section from experiments performed by the Stanford Linear Accelerator Center/Lawrence Berkeley Laboratory collaboration at the SLAC electron-positron colliding beam facility SPEAR were presented at the 1973 Irvine Conference.[6] Substantially the same data, but with reduced errors, were discussed by Richter[7] at the London Conference just a year ago. These measurements, spaced every 200 MeV in c.m. energy from 2.4 GeV to 4.8 GeV, strongly supported the earlier two points from CEA and indicated that R significantly increased over this energy range. In November of last year, while trying to understand certain variations in what was thought to be the smooth behavior of σ_T with energy, we discovered[8] the remarkably sharp peak in σ_T shown in Fig. 2 at 3.1 GeV right between two of the earlier measurements. This, of course, is the famous ψ or J resonance discovered independently in pp interactions at Brookhaven[9] and observed shortly after the initial discoveries at Frascati[10] and DESY.[11]

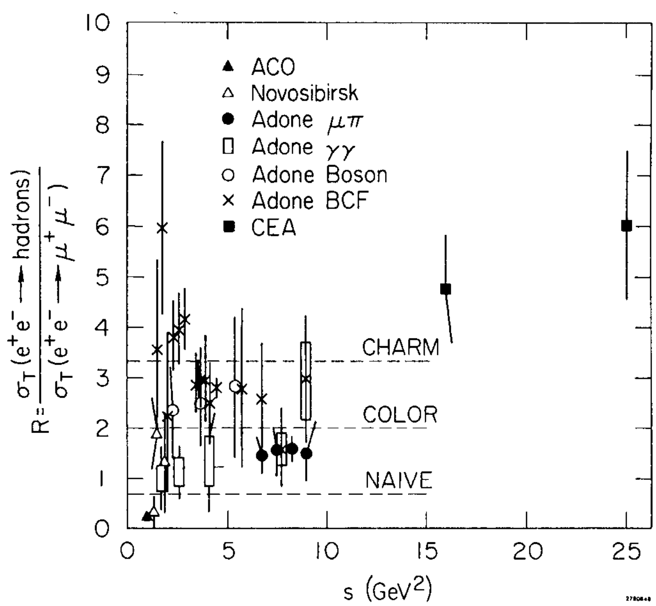

Fig. 1--$R = \sigma(e^+e^- \to \text{hadrons})/\sigma(e^+e^- \to \mu^+\mu^-)$ versus the square of the c.m. energy s. The ACO point is from Ref. 3; Novosibirsk points are from Ref. 4; Adone points are from Ref. 2; CEA points, from Ref. 5. The dashed lines represent the predictions of various quark models (see Ref. 19).

* Work supported by the U. S. Energy Research and Development Administration.

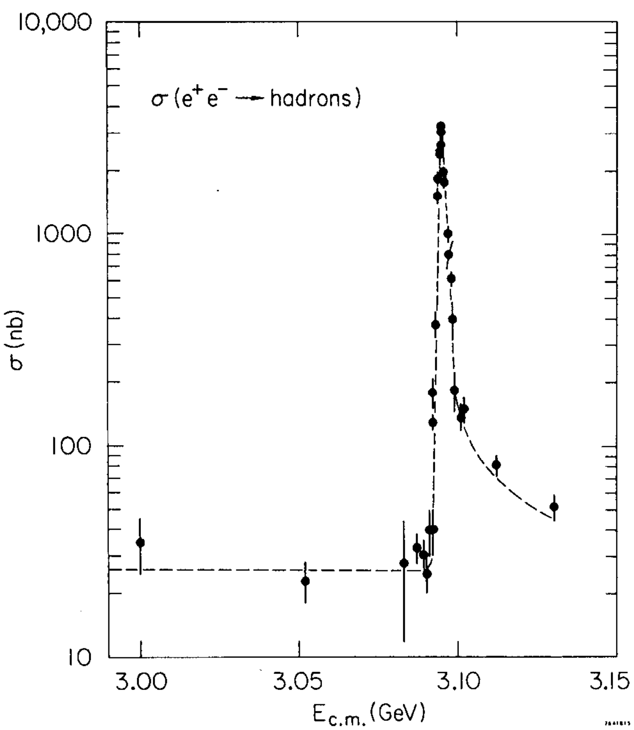

Fig. 2--Total hadronic cross section σ vs $E_{c.m.}$ in the vicinity of the $\psi(3095)$ resonance.

Within days a second narrow resonance was discovered at SPEAR[12] and suddenly our picture of the total hadronic cross section had changed dramatically.[13]

I shall now report on what we have learned about hadron production at SPEAR since the discovery of the new particles. This work is a product of the SLAC/LBL collaboration[14] using the SPEAR magnetic detector.

II. SPEAR MAGNETIC DETECTOR

The SPEAR magnetic detector, shown schematically in Fig. 3, is a 3-meter long, 3-meter diameter solenoid magnet with a 4 kG magnetic field parallel to the incident beam direction. The beams collide at the center of this detector over a volume a few centimeters long in the beam direction and a fraction of a millimeter wide in transverse dimensions. Particles emerging from the luminous region of the beams pass in sequence through a thin-walled vacuum chamber, cylindrical scintillation counters and multiwire proportional chambers immediately surrounding the vacuum chamber, a system of magnetostrictive spark chambers, an array of trigger time-of-flight scintillation counters, the magnet coil, an array of lead scintillator shower counters, the magnet return iron, and finally a set of muon identifying spark chambers. Two or more charged particles firing the vacuum chamber scintillation counter and trigger counters in coincidence with minimum ionizing signals from their associated shower counters were required to trigger the apparatus. The full momentum analysis, tracking, and particle identification capabilities of this device extend over 65% of 4π solid angle.

Two general categories of events were selected for the results presented here. Events having two oppositely charged prongs collinear within 10°, with momenta greater than 1/2 the incident beam energy, were identified as being electrodynamic; they arise from the reactions

$$e^+e^- \rightarrow e^+e^- \quad (1)$$

$$e^+e^- \rightarrow \mu^+\mu^- \quad . \quad (2)$$

Shower counter information was used to distinguish Bhabha scattering events (1) from muon pairs (2).

Events where three or more prongs formed a vertex within the luminous region were classified as multihadronic events if no collinear pair of tracks having large

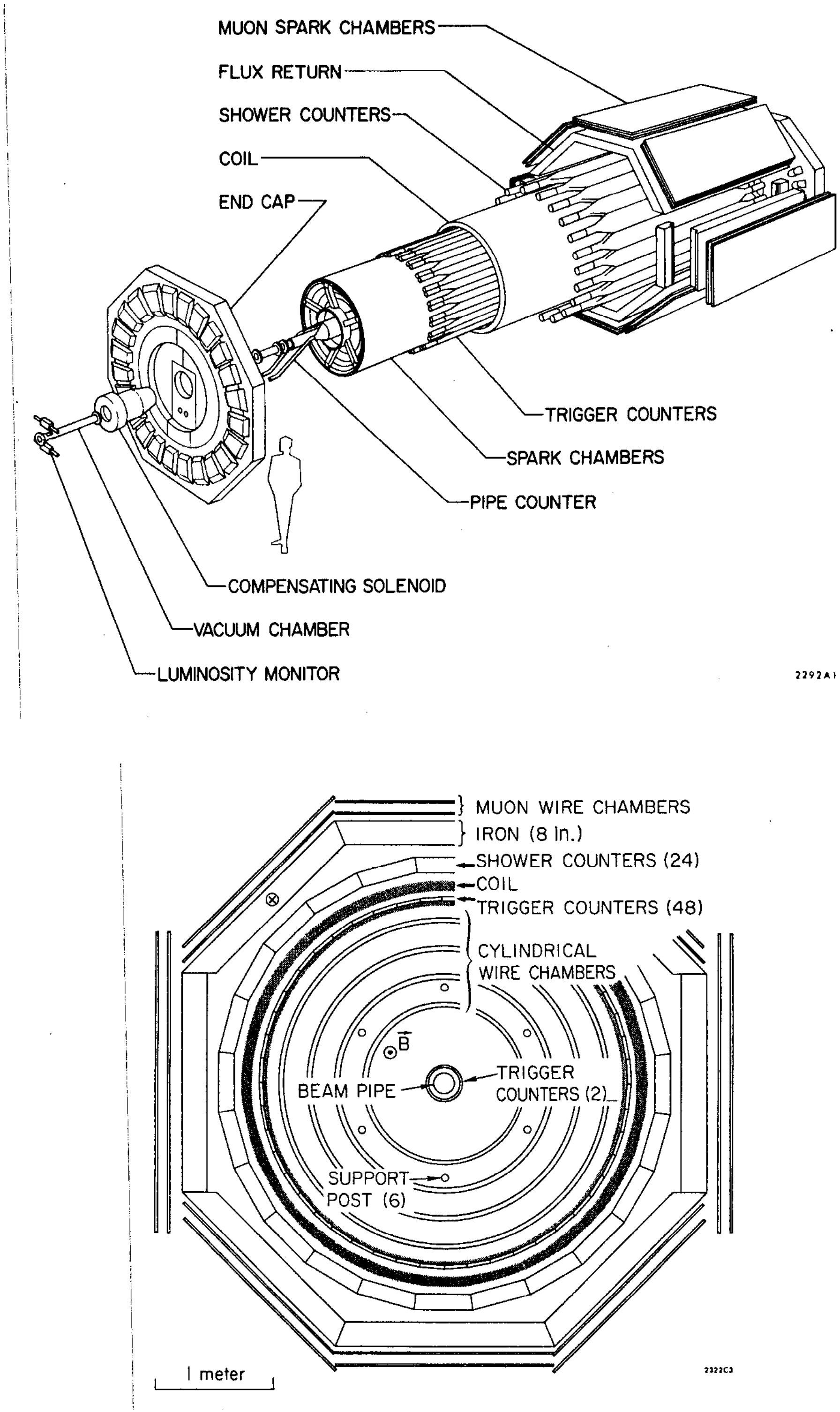

Fig. 3--Schematic diagrams of the SLAC/LBL magnetic detector showing major components.

shower counter pulse height (consistent with electrons) was present. Two prong events where the planes formed by the tracks and the incident beam direction were acoplanar by at least 20^{o} and where the momenta of both prongs were greater than 300 MeV/c were also included in the hadron event sample. The purpose of these cuts was to reject various electrodynamic background which could contaminate the hadron sample. Details of the SPEAR magnetic detector and event selection procedures are given in Refs. 13 and 15.

III. σ_{TOTAL}

The total hadronic cross section was obtained totaling up all the hadronic events and dividing by the integrated luminosity. Corrections were made to account for the less than complete solid angle acceptance of the detector, trigger biases, and cuts. A Monte Carlo simulation of the detector, with its known inefficiencies and analysis cuts, was used in conjunction with several plausible models of the multihadronic final states to calculate the efficiencies ϵ_{qp} for detecting events that were produced with p charged prongs and had q of these prongs observed in the apparatus. The observed charged multiplicity distribution is related to the produced charged multiplicity distribution through the ϵ_{qp}:

$$N_q = \sum_p \epsilon_{qp} \tilde{N}_p \tag{3}$$

where N_q is the number of events detected with q-charged prongs and $\tilde{N}_p$ is the number of events produced having p-charged prongs. Knowing the efficiencies ϵ_{qp}, these equations can be "unfolded" by a maximum likelihood method to yield the produced multiplicity distribution. The average detection efficiency $\bar{\epsilon}$ is defined:

$$\bar{\epsilon} = \frac{\sum_q N_q}{\sum_p \tilde{N}_p} \tag{4}$$

Values for $\bar{\epsilon}$ have been obtained by the unfold procedure for our published data[13] and at selected higher energies. These are shown in Fig. 4. The curve in Fig. 4 is our estimate of $\bar{\epsilon}$ at other energies, assuming $\bar{\epsilon}$ to be a smooth function of center-of-mass energy, $E_{c.m.}$. This "smooth" average detection efficiency was used to correct the preliminary hadronic cross section data being presented here. The older published points use "unfolded" average detection efficiencies.

Finally, the total hadronic cross section is given by the following:

$$\sigma_T = \frac{\sum_q N_q}{\bar{\epsilon} \int \mathscr{L} dt} \tag{5}$$

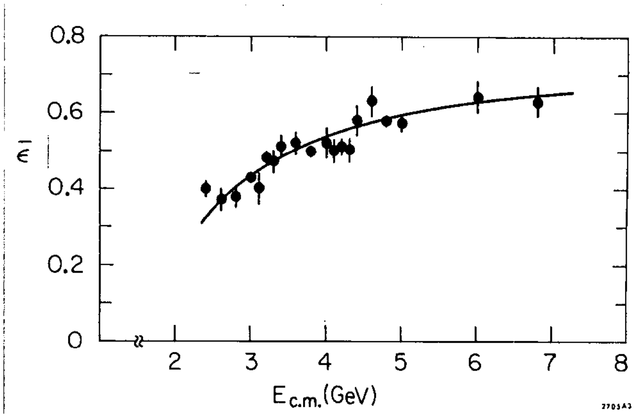

Fig. 4--Average detection efficiency $\bar{\epsilon}$ vs $E_{c.m.}$. The points are determined by the "unfold" procedure. The curve is the so-called "smooth" efficiency.

where the integrated luminosity $\int \mathscr{L}dt$ was derived from Bhabha scattering events observed in the magnetic detector.

With the discovery of the narrow states $\psi(3095)$ and $\psi(3684)$, it became imperative to perform a systematic search for other such states. A scanning procedure was developed whereby the energy of SPEAR could be automatically stepped in center-of-mass increments of approximately 2 MeV between short data runs at each energy. The runs would last a few minutes, the time necessary to collect two or three hadronic events on average. The magnetic detector and SPEAR were tied to an elaborate computer system which provided cross section results in real time to aid in the execution of the experiment. We have published the results of these scans up to an energy of 5.9 GeV.[16] They are shown in Fig. 5. Recently we have completed the scan up to an energy of 7.6 GeV, as shown in Fig. 6. Aside from the $\psi(3095)$ and $\psi(3684)$, no new narrow resonances have been discovered. The limits we can set on the integrated areas of possible resonances that escape detection are given in Table I.

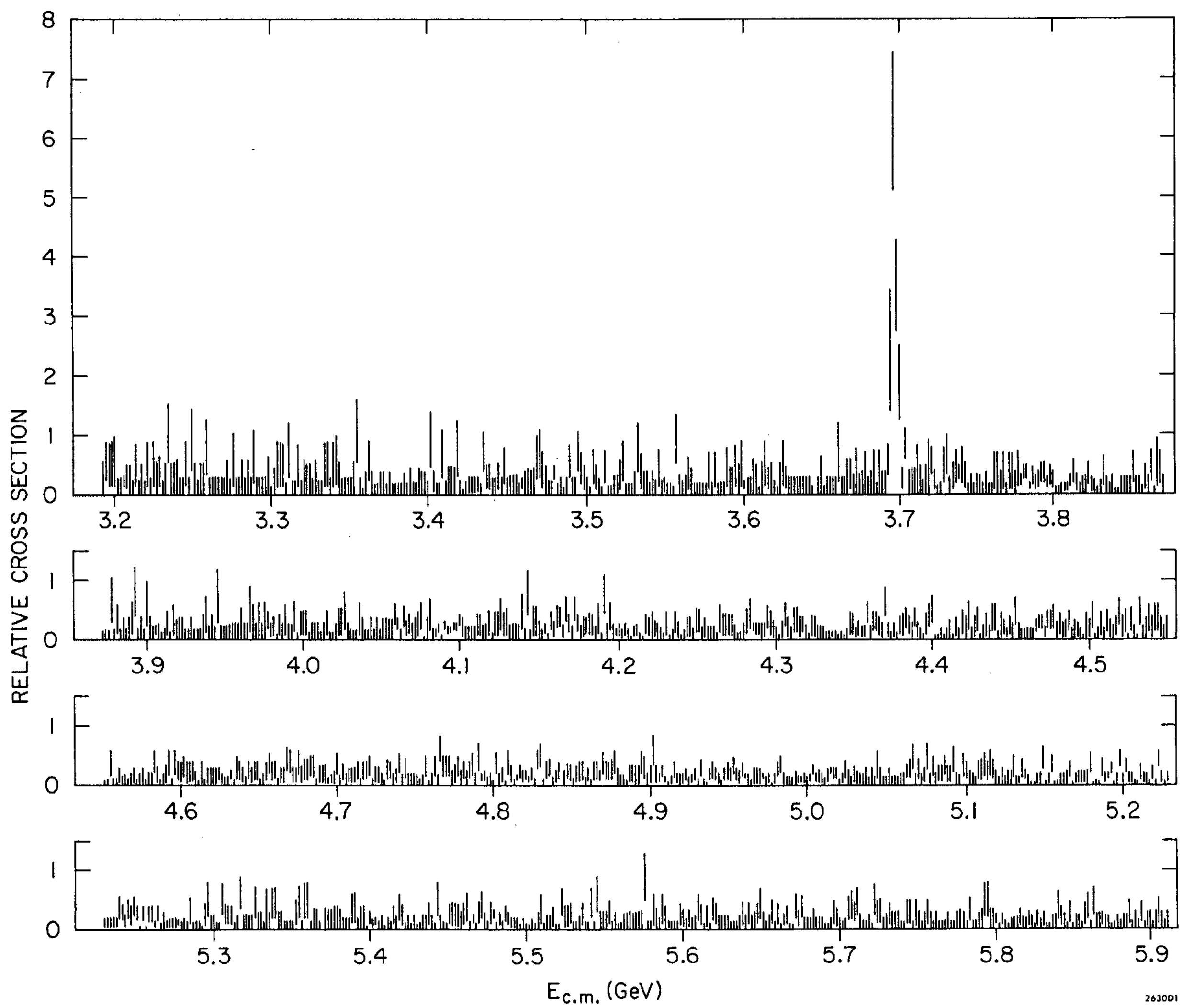

Fig. 5--Total hadronic cross section vs $E_{c.m.}$ in fine steps over the range $3.2 \text{ GeV} \leq E_{c.m.} \leq 5.9 \text{ GeV}$. The clear peak is the $\psi(3684)$.

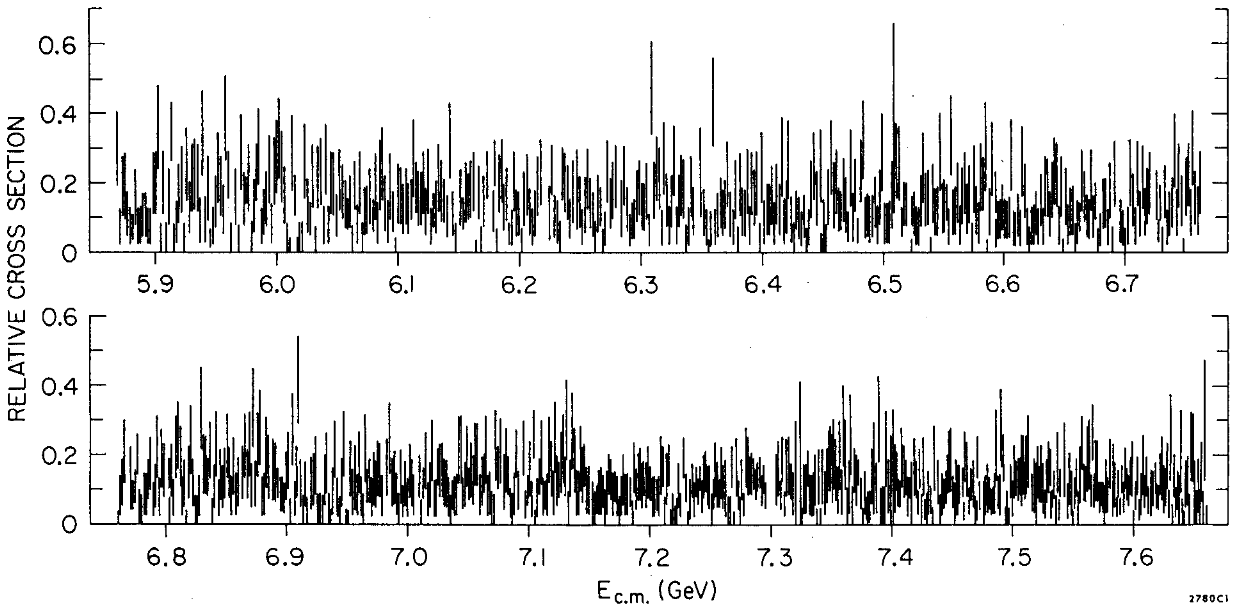

Fig. 6--Total hadronic cross section vs $E_{c.m.}$ in fine steps over the range 5.9 GeV $\leq E_{c.m.} \leq$ 7.6 GeV.

TABLE I

Results of the search for narrow resonances. Upper limits (90% confidence level) for the radiatively corrected integrated cross section of a possible narrow resonance. The width of this resonance is assumed to be small compared to the mass resolution.

Mass Range (GeV)	Limit on $\int \sigma_H \, dE_{c.m.}$ (nb MeV)
3.20 → 3.50	970
3.50 → 3.69	780
3.72 → 4.00	850
4.00 → 4.40	620
4.40 → 4.90	580
4.90 → 5.40	780
5.40 → 5.90	800
5.90 → 7.60	450

This method of scanning is most sensitive to resonances having intrinsic widths smaller than can be resolved at SPEAR. The c.m. energy resolution is determined by the spread in beam energies arising from fluctuations in the synchrotron radiation process. The c.m. energy spread is energy-dependent with typical values of approximately 1 MeV. Thus, additional resonances in the mass range 3.0 to 7.6 GeV/c^2

having widths of order 1 MeV or less are limited to integrated areas which are a small fraction of those of the ψ resonances. Equivalently, their partial widths to electron pairs must be less than 500 to 1000 electron volts over this mass range.

To search for structure on a broader scale we have measured σ_T at many energies with much greater precision than in the fine scan. The results of this program are shown in Fig. 7. Both our previously published data[13] up to 5 GeV and new preliminary results using the "smooth" detection efficiency discussed earlier are given.

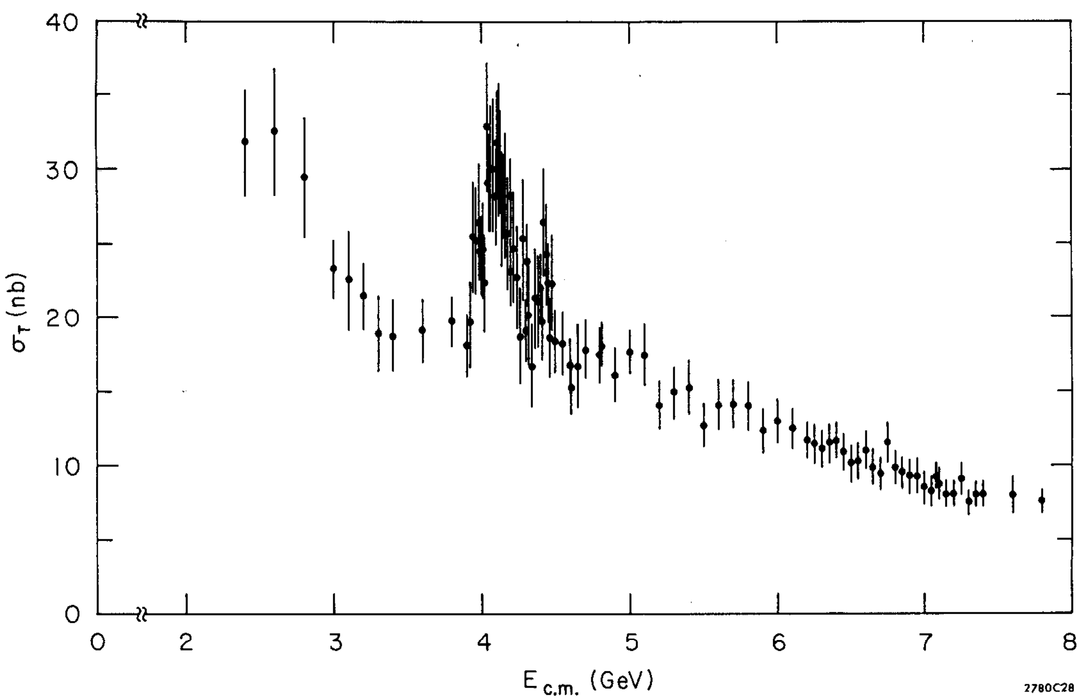

Fig. 7--Total hadronic cross section vs $E_{c.m.}$ in coarse steps. Combination of published results[13] and new preliminary results from SLAC/LBL collaboration. Radiative tails of the ψ resonances have been removed.

The new data were corrected for beam gas backgrounds ($\lesssim 5\%$) and contamination due to electrodynamic final states arising from two-photon processes[17] ($< 2\%$). Radiative corrections[18] have been applied to remove the tails of the narrow ψ resonances; they also take into account the smooth behavior of the σ_T away from the resonances. The error bars include statistical errors and our estimate of point-to-point systematic errors ($\pm$ 8% on the published results, $\pm$ 10% on new results). The overall normalization uncertainty is $\pm$ 10% and a further, smooth variation as large as 15% from lowest energy to highest could arise from systematic errors in $\bar{\epsilon}$.

From Fig. 7 we see that σ_T generally falls with increasing c.m. energy except in the 4 GeV region, where it exhibits some very interesting structure. The ratio R of σ_T to the muon pair cross section is presented in Fig. 8. Below 3.5 GeV, R is approximately constant, with a value around 2.5. Above 5 GeV, R is again roughly constant, but at a level approximately twice that of the lower energy scaling region.

Between these two regions in R, there is a very complicated transition region with indications of a richness of structure that we are only beginning to resolve.

A more detailed view of R in the 4 GeV region is presented in Fig. 9. The new and more extensive preliminary results (closed points) have a different impression from that of our previously published data (open points). The main features in this region are the broad structure centered near 4.1 GeV and strong indications of another resonance at 4.4 GeV having a width of about 50 MeV. The 4.1 GeV bump has a somewhat peculiar looking low energy edge that may indicate even more structure in this region. Clearly, a great deal more experimental effort is required to untangle this very complicated and interesting region.

The dramatic doubling of R over the energy range of this experiment suggests that new hadronic degrees of freedom may be opening in the 4 GeV region. The low energy region where

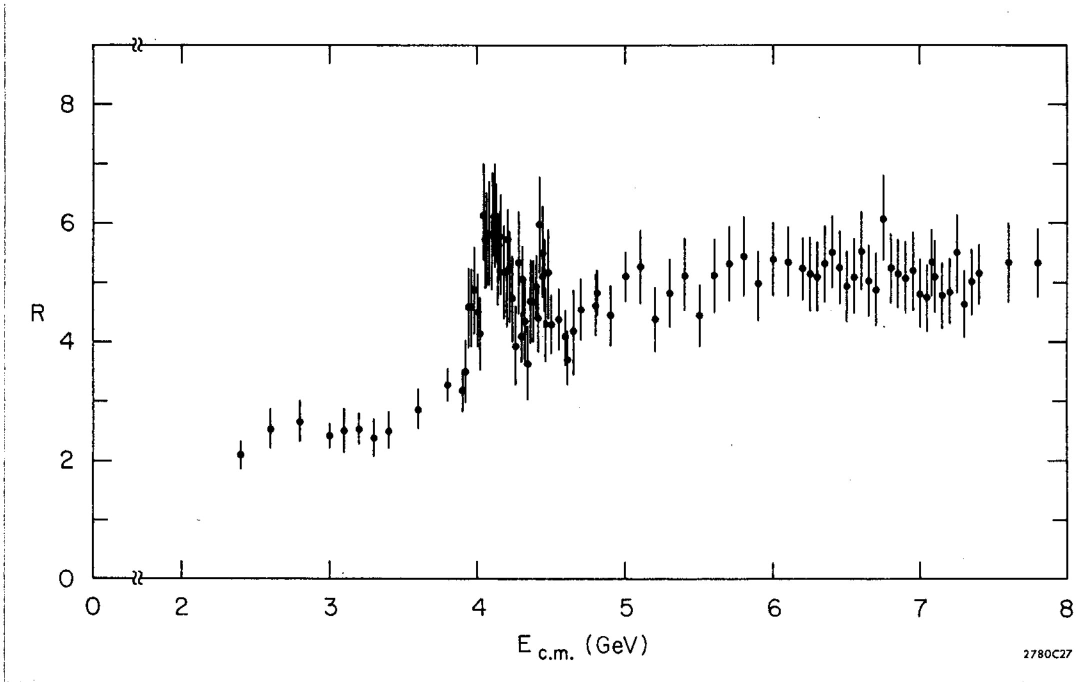

Fig. 8--R versus $E_{c.m.}$ in coarse steps. Combination of published results[13] and new preliminary results from SLAC/LBL collaboration.

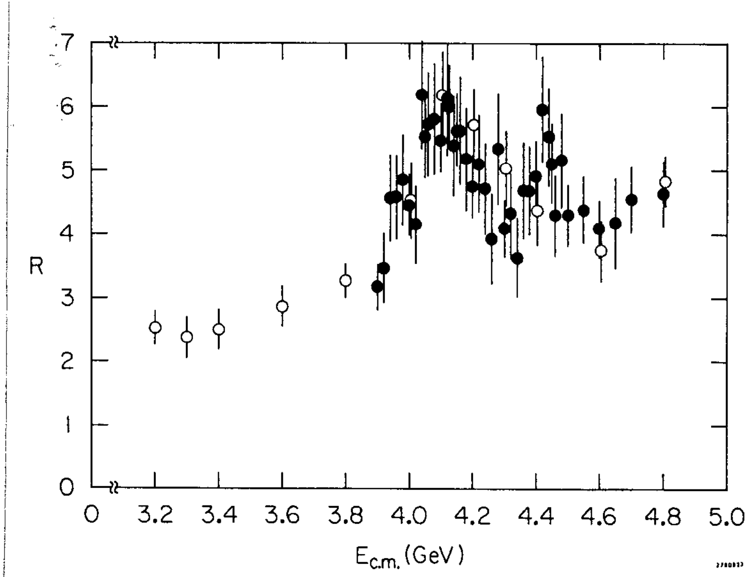

Fig. 9--R versus $E_{c.m.}$ in the 4 GeV region. Open points are from Ref. 13, closed points are new preliminary results.

R ≃ 2.5 is compatible with quark models[19] having 3 "flavors" of Gell-Mann/Zweig quarks in three colors that predict R = 2. The increase in R may indicate the presence of new processes which are adding 2 to 3 units of R to the "old physics" represented by R ≃ 2.5. The interesting and challenging experimental question is whether there are fundamentally new processes occurring above 4 GeV and, if so, what distinguishes the "new" physics from the "old".

IV. MEAN CHARGED MULTIPLICITY AND ENERGY

One place to look for differences between new and old physics is in various moments of the data. The mean charged multiplicity $\langle n_{ch}\rangle$, a direct by-product of the unfold procedure which gave $\bar{\epsilon}$, is plotted in Fig. 10 versus the logarithm of the c.m. energy. The data are consistent with a logarithmic growth in charged multiplicity; a power law or some other slow growth cannot be ruled out. This behavior is reminiscent of the multiplicity growth in many other reactions at similar energies. There is no evidence for changes in this behavior in the 4 GeV region, although the uncertainties are rather large and could obscure important effects.

The mean energy of the observed tracks $\langle E_{track}\rangle$ as a function of c.m. energy is given in Fig. 11. For this analysis, only three or more prong events were considered and every track was assigned a pion mass in the calculation of its energy. In this case there is some evidence for a change in the overall behavior near 4 GeV. $\langle E_{track}\rangle$ rises from the lowest c.m. energies covered until nearly 4 GeV, where it levels off before beginning to rise again. This leveling of $\langle E_{track}\rangle$ may indicate a small yet sudden increase in the total (charged + neutral) multiplicity near 4 GeV.

The mean fraction of c.m. energy appearing in charged particles is shown in Fig. 12. Again, three or more prong events were used and pion masses were assigned to all tracks. The data have been corrected for the expected losses of charged particles

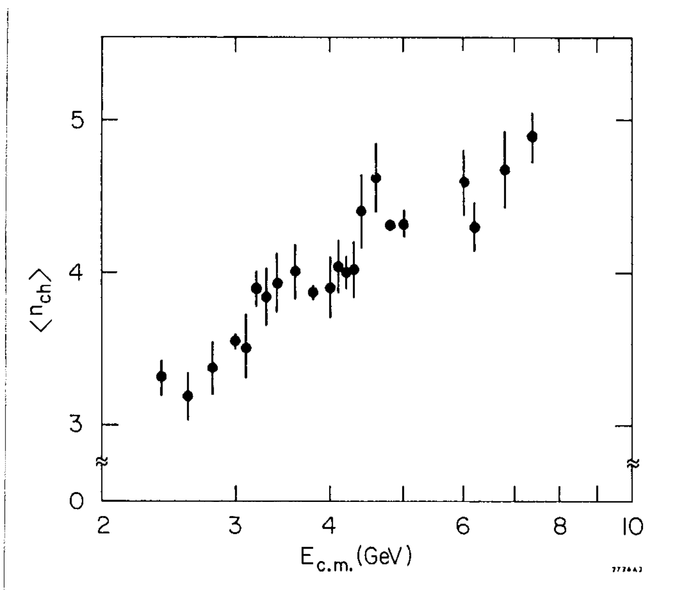

Fig. 10--Mean charged multiplicity $\langle n_{ch}\rangle$ vs $E_{c.m.}$.

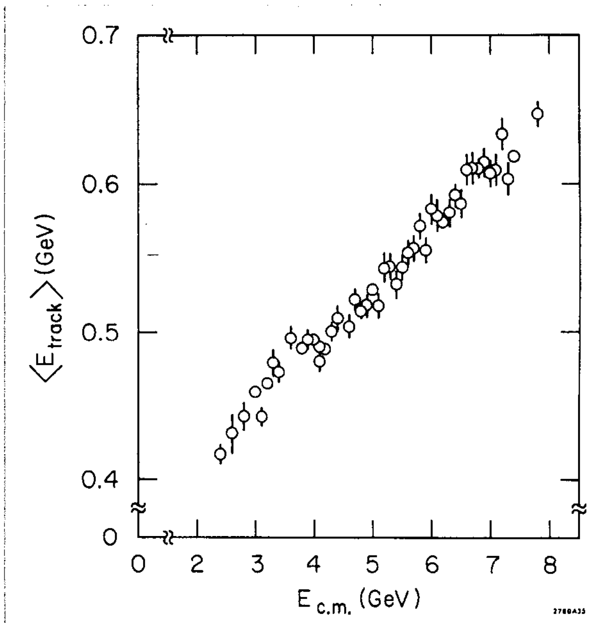

Fig. 11--Mean energy per track (assuming pion mass) $\langle E_{track}\rangle$ vs $E_{c.m.}$ for ≥ 3 prong events.

due to trigger biases and solid angle acceptance by means of a Monte Carlo calculation. The correction factor is a smooth function of c.m. energy. An important feature of Fig. 12 is the fact that the charged energy fraction is less than its naively expected value of 2/3 at all energies. It falls from 0.6 to 0.5 from lowest to highest c.m. energies covered in this experiment and may be leveling off at 0.5. The fact that the charged energy fraction is 0.6 rather than 0.67 at the lowest energies is probably a consequence of the production of heavy particles such as nucleons, kaons, and etas, in addition to pions. Why it should fall with increasing c.m. energy is not so easily understood. There is a hint, albeit a feeble one, that the charged energy fraction has a discontinuity in the 4 GeV region.

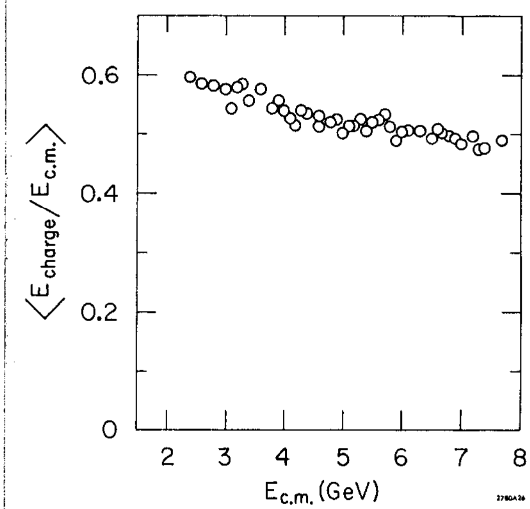

Fig. 12--Average fraction of total c.m. energy appearing in charged particles vs $E_{c.m.}$. Pion masses are assumed. The data have been corrected for acceptance and analysis losses.

V. INCLUSIVE MOMENTUM SPECTRA

The SPEAR magnetic detector allows us to measure the momentum p of charged particles with a fractional resolution of

$$\frac{\delta p}{p} \approx 0.05 \times p \quad (\mathrm{GeV}) \tag{6}$$

over 65% of a solid angle. We have studied single particle inclusive momentum spectra with the large samples of 3 or more prong hadronic events available at selected c.m. energies. The data are presented as a function of the scaling variable x defined as

$$x \equiv 2p/E_{c.m.} \tag{7}$$

This particular choice of scaling variable was motivated by the fact that we measure p and do not attempt to identify the type of hadron. The data have been corrected for beam-gas background and the radiative tail of $\psi(3684)$ has been removed from the 3.8 GeV data. Monte Carlo corrections have been applied to the spectra to give our best estimate of the momentum spectra integrated over the full 4π solid angle; the data have polar angles in the range $-0.7 < \cos\theta < 0.7$. The overall magnitude of the correction factors closely follows the energy dependence of the average detection efficiency discussed above. The shape of the correction as a function of x is roughly independent of $E_{c.m.}$ and slowly varies with x in the interval $0.1 < x < 0.8$.

The first inclusive quantity we study is s $d\sigma/dx$. The sum rule for this distribution may be written

$$\int s\frac{d\sigma}{dx}dx = s\,\sigma_T \langle n_{ch}\rangle \tag{8}$$

$$\propto R\langle n_{ch}\rangle$$

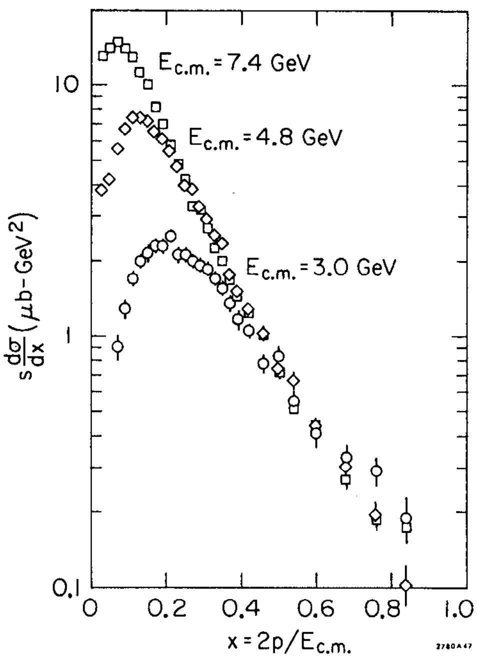

Fig. 13--s $d\sigma/dx$ vs x for $E_{c.m.}$ = 3.0 GeV, 4.8 GeV, and 7.4 GeV. $x \equiv 2p/E_{c.m.}$.

The sum rule indicates that the area under s $d\sigma/dx$ will increase with increasing c.m. energy because we already know that both the mean charged multiplicity and R increase over the energy range studied in our experiment. In Fig. 13 s $d\sigma/dx$ is plotted versus x for $E_{c.m.}$ = 3.0, 4.8, and 7.4 GeV. Our uncertainty in these spectra (and in the spectra presented in Figs. 14 and 15) is greatest at the lowest and highest values of x because of the low statistics, the fact that the Monte Carlo corrections are largest in these regions, and the fact that the momentum resolution is worse and probably non-gaussian at high momenta. The error bars shown in Figures 13, 14, and 15 are statistical only. Systematic errors could lead to 20% changes in s $d\sigma/dx$ at the highest and lowest values of x with smooth variation across the available values of x.

The spectra for all three energies shown in Fig. 13 rise sharply at small values of x, peak at relatively low x, then fall with increasing x. The rise at small x is expected because of the increase in available phase space. The areas under the data in Fig. 13 increase significantly with increasing $E_{c.m.}$ as expected from Eq. (8). The interesting point is that almost all of the increase in area is in the low x region ($x < 0.5$); above $x = 0.5$ the spectra for the three different energies are equal within experimental error, and thus are consistent with Bjorken scaling.[20]

To study the question of Bjorken scaling in the inclusive spectra more critically, s $d\sigma/dx$ is plotted versus $E_{c.m.}$ for several x intervals in Fig. 14. Bjorken scaling implies that s $d\sigma/dx$ should not change with $E_{c.m.}$ at fixed values of x. In the lowest x interval near $x = 0.1$, scaling is badly broken. By $x = 0.2$, however, the data are more or less constant with c.m. energy for $E_{c.m.}$ greater than 4 GeV. For $x \geq 0.4$, the data are consistent with Bjorken scaling over the entire energy range with the possible exception of data taken in the 4 GeV region.

Another way to view the inclusive momentum distribution of hadrons is through the quantity $\frac{1}{\sigma_{\mu\mu}} x\frac{d\sigma}{dx}$. This distribution function has the following approximate yet convenient sum rule.

$$\frac{1}{\sigma_{\mu\mu}} \int x\frac{d\sigma}{dx}dx = \frac{1}{\sigma_{\mu\mu}} \int \left(\frac{p}{E}\right)^2 E\frac{d\sigma}{dE}dE \simeq 2 f_{ch} R \tag{9}$$

where E is the hadron energy and f_{ch} is the fraction of c.m. energy appearing in charged particles, the same quantity as plotted in Fig. 12. We have measured $\frac{1}{\sigma_{\mu\mu}} x \frac{d\sigma}{dx}$ at several c.m. energies and the results are presented in Fig. 15. Again, the approximate Bjorken scaling noted previously is apparent, particularly at the

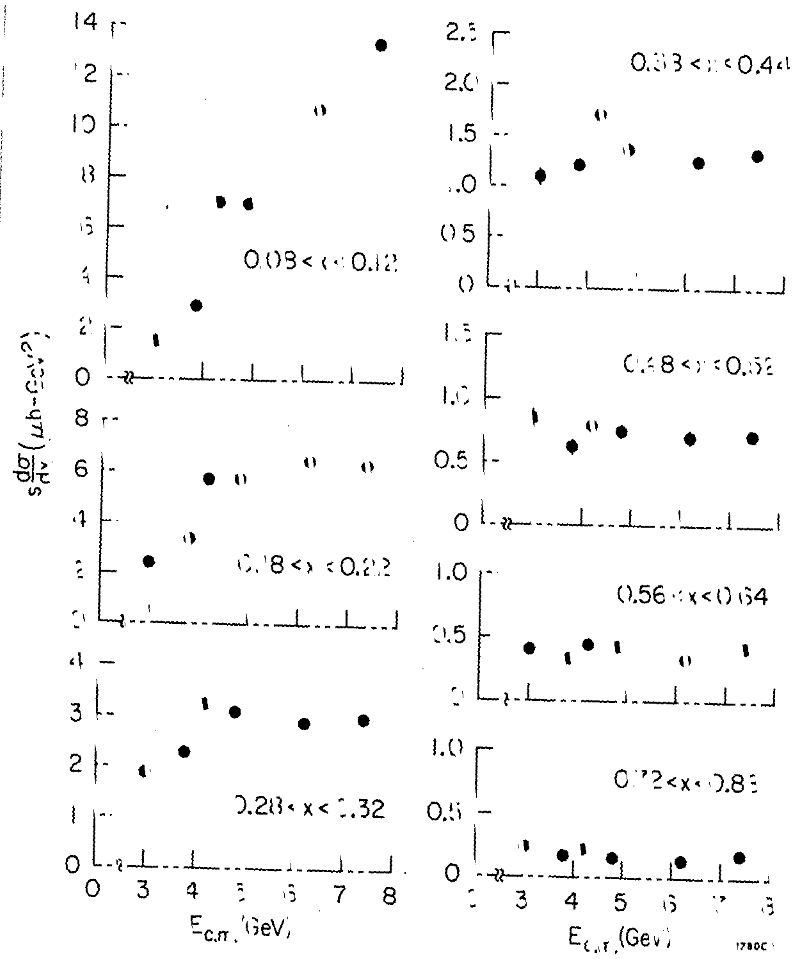

Fig. 14--s $d\sigma/dx$ vs $E_{c.m.}$ for various x intervals.

highest energies. In fact, one can imagine an envelope which would represent $\frac{s}{\sigma_{\mu\mu}}\,x\,\frac{d\sigma}{dx}$ at asymptotically high energies. The present data simply may be low energy approximations to the asymptotic curve where phase space corrections modify the low x behavior. The data taken in the 4 GeV region do not appear to fall on some universal curve, however. In Fig. 15, they indicate a small excess of prongs at intermediate values of x. This "bulge" for $0.3 \lesssim x \lesssim 0.5$ may be a clue to understanding the question posed above concerning the difference between "old" and "new" physics; present experimental uncertainties preclude a definite conclusion.

VI. ANGULAR DISTRIBUTION OF HADRONS

Electron-positron annihilation into hadrons is expected to proceed through the one-photon intermediate state, thus greatly simplifying the angular distribution of produced particles. The most general angular distribution for any single photon annihilation process can be written[19]

$$\frac{d\sigma}{d\Omega} = \sigma_T + \sigma_L + (\sigma_T - \sigma_L)(\cos^2\theta + P^2\sin^2\theta\cos 2\phi) \qquad (10)$$

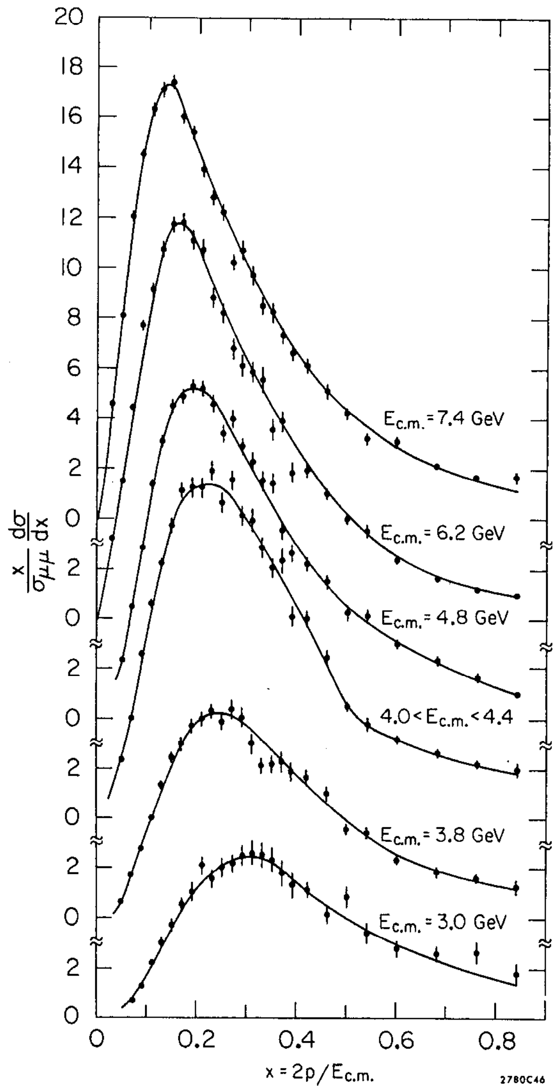

Fig. 15--$(x/\sigma_{\mu\mu})(d\sigma/dx)$ vs x for for various $E_{c.m.}$.

The inclusive polar angle distributions for three or more prong events as observed in the magnetic detector are shown in Fig. 16. The tracks are seen to be quite uniformly distributed in cos θ; the falloff in the number of prongs in the outermost bins is due to acceptance losses. Prongs with $x > 0.3$ at $E_{c.m.} = 7.4$ GeV show strong evidence for a $\cos^2\theta$ term while the low x data do not. At $E_{c.m.} = 4.8$ GeV the data are inconclusive; prongs with $x > 0.3$ are compatible with a positive value of α but

where θ is the polar angle measured with respect to the incident e^+ direction. ϕ is the azimuthal angle measured from the plane of the storage ring, P is the transverse polarization of the incident beams (discussed below). The "physics" is contained in the functions σ_T, σ_L which are non-negative functions of the type of particle being observed, its energy and the c.m. energy. σ_T measures the coupling to states of net helicity one along the direction given by θ and ϕ; σ_L measures the coupling to states of 0 net helicity in this direction. It is convenient to define a quantity α

$$\alpha = \frac{\sigma_T - \sigma_L}{\sigma_T + \sigma_L} . \qquad (11)$$

So the general angular distribution integrated over azimuthal angle has the form

$$\frac{d\sigma}{d\cos\theta} \propto 1 + \alpha\cos^2\theta \quad (-1 \le \alpha \le 1) \qquad (12)$$

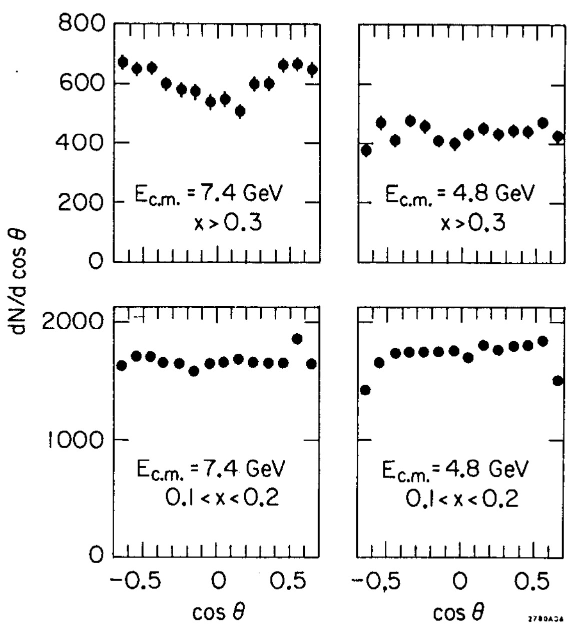

Fig. 16--cos θ distributions for $\geq$ 3-prong hadronic events at $E_{c.m.} = 7.4$ GeV and 4.8 GeV for various ranges of x. cos θ bins are 0.1 units wide.

they poorly determine α. This points out the difficulty of determining α from the polar angle distribution alone because of the relatively small range of $\cos^2\theta$ covered by the magnetic detector. Fortunately, we have available another means for studying the parameter α, namely through the polarization dependent term in Eq. (10).

As the stored beams circulate and interact with the synchrotron radiation field, they become polarized transversely to their direction of motion.[22,23] Positrons (electrons) are polarized parallel (antiparallel) to the guide magnetic field. The characteristic time T_{pol} which governs the buildup of polarization depends on the radius and bending field of the storage ring. For SPEAR, T_{pol} is given by

$$T_{pol} \simeq 15 \left(\frac{7.4}{E_{c.m.}}\right)^5 \text{ minutes.} \tag{13}$$

The theoretical asymptotic polarization is $P_0 = 8\sqrt{3}/15 \simeq 0.924$; however, the asymptotic polarization measured at SPEAR[24] appears to be somewhat less, $P_0 \simeq 0.8$.

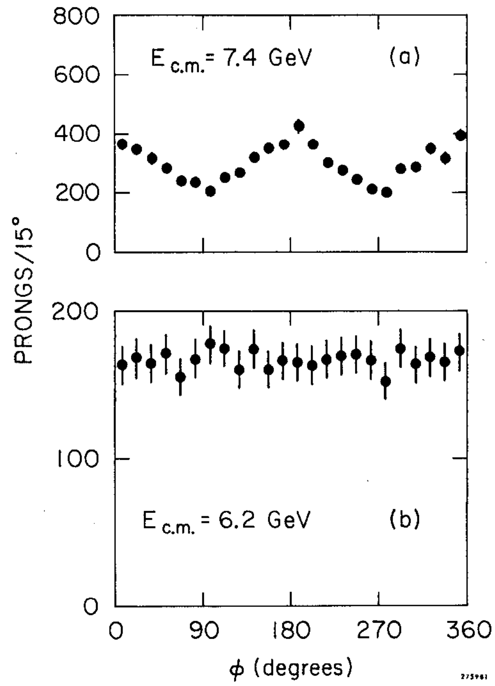

Fig. 17--Azimuthal distribution of prongs with $x > 0.3$ and $|\cos\theta| \leq 0.6$ for $E_{c.m.} = 6.2$ GeV, 7.4 GeV. $\phi = 0$ is the horizontal plane.

Inclusive azimuthal distributions for particles with $x > 0.3$ and $|\cos\theta| < 0.6$ are shown in Fig. 17 for the two c.m. energies 7.4 GeV and 6.2 GeV. In the 7.4 GeV results there is unmistakable evidence for a strong $\cos 2\phi$ term as would be expected from Eq. (10). The 6.2 GeV azimuthal distribution, however, is completely flat. This is an example of a depolarizing resonance[23] of the storage ring. At the nominal 6.2 GeV setting of the SPEAR energy, the spins of electrons and positrons precess an integral number of turns (7 in this case) per orbit due to their normal "g-2" motion. Thus, guide field errors, which have little effect on spin motion off resonance, add coherently and destroy the beam polarization at the resonant energy. The 6.2 GeV results provide a convenient control sample for studying possible asymmetries in the apparatus. We find no significant azimuthal asymmetry in the apparatus.

The inclusive hadron angular distribution (in θ and ϕ) at $E_{c.m.} = 7.4$ GeV was fitted to the functional form of Eq. (10) by a maximum likelihood method in order to determine the functions σ_T and σ_L. The average value of P^2 for these data was determined by a maximum likelihood fit to the muon pair data collected simultaneously. The value obtained is $P^2 = 0.46 \pm 0.05$. Figure 18 shows the relative contributions of σ_T and σ_L as determined from the fits. At low x, σ_T and σ_L are approximately equal while above $x = 0.2$ the helicity one or transverse production dominates. This transverse coupling displayed by the hadrons is characteristic of the production of pairs of spin-$\frac{1}{2}$ particles as opposed to pion pair production, for example. It is what would be expected in the spin-$\frac{1}{2}$ parton model[25] where hadrons seen in the final state are emitted by the partons. A more complete discussion of these results is contained in our recent publication.[26]

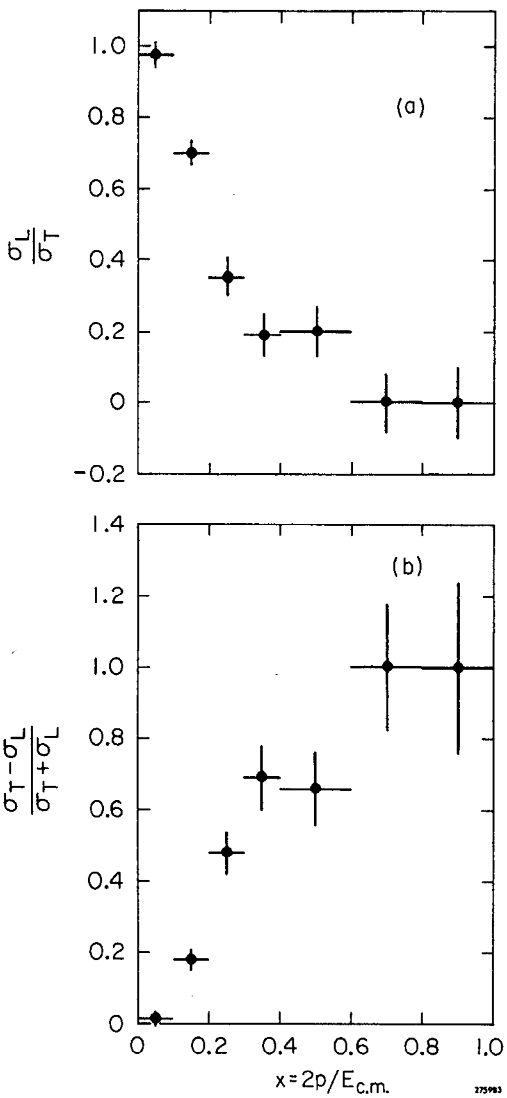

Fig. 18--(a) σ_L/σ_T vs x at $E_{c.m.} = 7.4$ GeV. (b) $(\sigma_T - \sigma_L)/(\sigma_T+\sigma_L)$ vs x at $E_{c.m.} = 7.4$ GeV.

VII. JET STRUCTURE

We have seen that the mean charged multiplicity slowly grows with energy, perhaps like log (s). Thus we expect a nearly linear dependence of the mean energy per particle with c.m. energy and this is consistent with the approximate Bjorken scaling noted previously. This kind of behavior is reminiscent of conventional hadron physics and suggests[27] that the invariant cross section for inclusive hadron production $E\, d\sigma/d^3p$ may be factorizable into a scaling part for momentum parallel to some preferred axis and a part limiting the momentum perpendicular to that axis. The difference between annihilation and conventional hadron collisions is, of course, that in the annihilation case hadrons are produced through the single photon intermediate state. Therefore, a preferred or "jet" axis cannot be the incident beam direction as in hadron collisions, but must have an angular distribution of the form given by Eq. (10). Nevertheless, what characterizes jet structure in e^+e^- annihilation is the fact that momentum perpendicular to some axis is limited.

To find jets, we searched 3 or more prong hadronic events for that axis which minimizes the sum of squares of momenta perpendicular to it. A discussion of the procedures involved is given in our recent publication.[28] For each event, a parameter called the sphericity S was computed. S is a measure of the jetlike character of the event and is defined by

$$S \equiv \frac{3\sum_i p_{\perp i}^2}{2\sum_i p_i^2} \qquad (14)$$

where the summation is over all prongs observed in the event, p_i is the prong momentum, and $p_{\perp i}$ is the momentum perpendicular to the jet axis. S is bounded between 0 and 1; events with small S are jetlike, events with large S are more like balloons. Sphericity distributions for data taken at three different incident beam energies are given in Fig. 19.

The next step was to compare sphericity distributions for the data with various models of final states. Two models, an invariant phase space model and a jet model which modified phase space to give limited transverse momentum, were used in Monte Carlo simulations of the detector. In both models, charged and neutral pions were produced; parameters of the models were adjusted to best represent observed properties of the final states. The mean value of $p_\perp$ used in the jet model was 315 MeV/c at all beam energies; this value was determined by a fit to the 7.4 GeV data.

The detected sphericity distributions for the models are presented with the data in Fig. 19. At $E_{c.m.} = 3$ GeV, both models agree with the data, while at the higher energies the jet model is preferred. At the higher energies, the phase space model poorly reproduces the inclusive momentum spectrum for $x > 0.4$. Therefore, Fig. 19d shows the S distribution at $E_{c.m.} = 7.4$ GeV for those events in which no particle has $x > 0.4$. Again, the data are well represented by the simple jet model and disagree with the phase space model. The mean sphericity for events as a function $E_{c.m.}$ is compared with predictions of

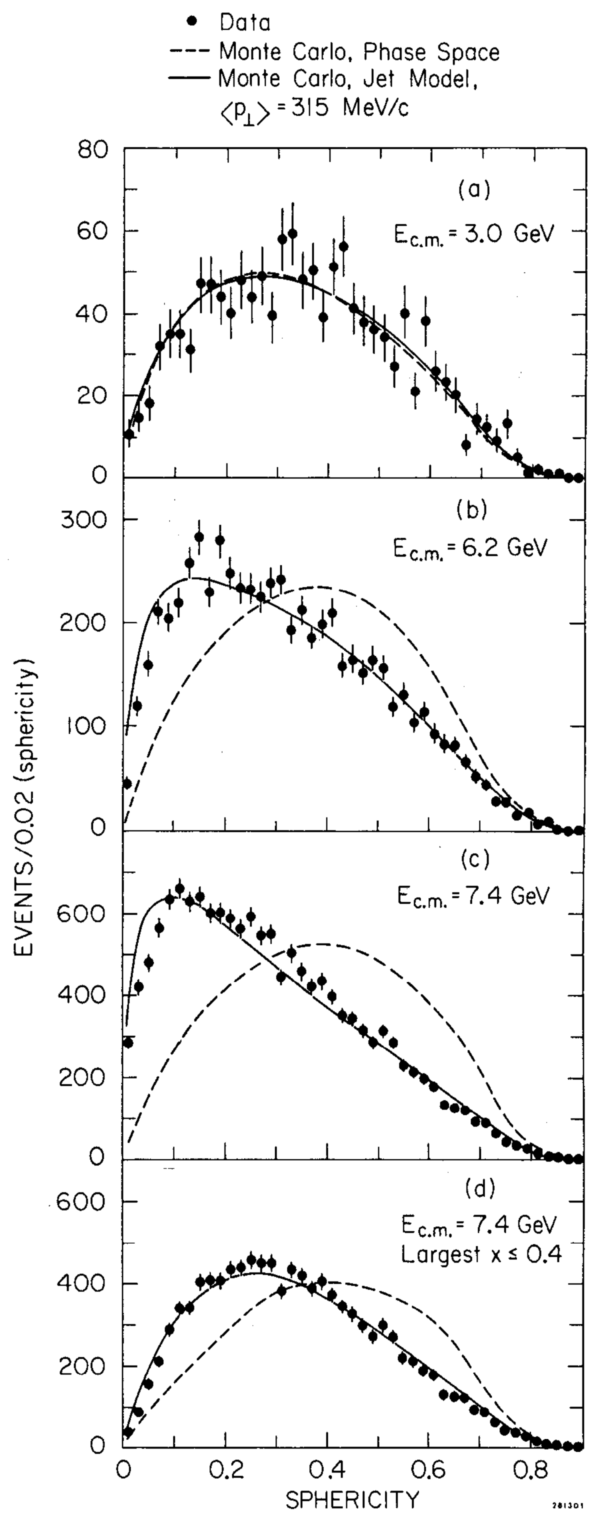

Fig. 19--Sphericity distributions for ≥ 3 prong hadronic events at various c.m. energies. The solid curves are the jet model (with $< p_\perp > = 315$ MeV/c) predictions; dashed curves are the invariant phase space Monte Carlo fits. In (d), only those events where all prongs have $x < 0.4$ were used.

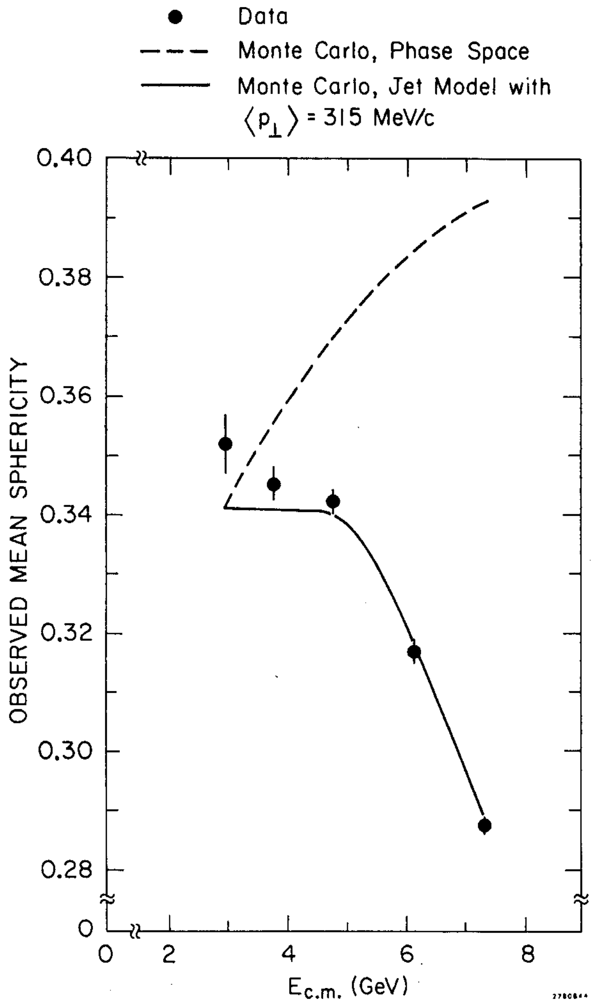

Fig. 20--Mean sphericity vs $E_{c.m.}$. The solid curve is the jet model result with $< p_\perp > = 315$ MeV/c. The dashed curve is the invariant phase space prediction.

the two models in Fig. 20. Below 4 GeV both models are consistent with the data, while at higher energies the jet model agrees with the data and the phase space model is definitely ruled out.

In these sphericity distributions, we are seeing a multiparticle correlation that cannot be explained by energy-momentum conservation alone. This correlation may be directly related to the mechanisms which give rise to the Bjorken scaling and limited multiplicity growth discussed above. Operationally, we find it is much easier to obtain satisfactory fits to observed properties of final states, such as momentum spectra, with the jet model than with the phase space model.

The inclusive angular distribution of hadrons at $E_{c.m.} = 7.4$ GeV is also well represented by the jet model. The angular distribution of the observed jet axis shows an azimuthal asymmetry of the form given by Eq. (10). From this we deduced that the angular distribution of the produced jet axis is described by $\alpha = 0.78 \pm 0.12$ where α is defined by Eq. (11). The hadrons emerging from jets with this angular distribution would display momentum dependent values of α as shown by the shaded curve in Fig. 21.

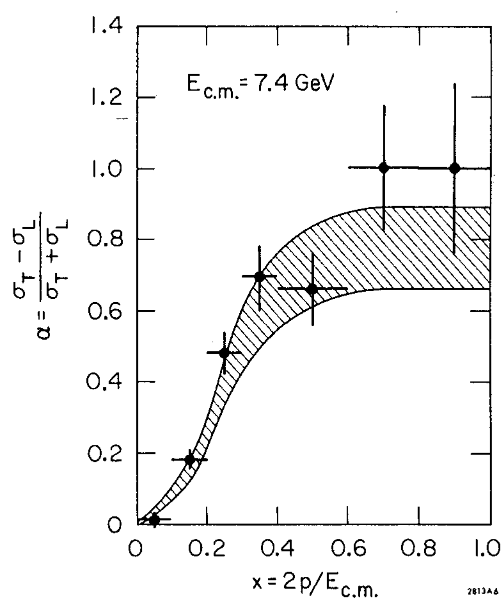

Fig. 21--α vs x at $E_{c.m.} = 7.4$ GeV. The data are the same as Fig. 18. The shaded curve is the jet model prediction with $\alpha_{jet} = 0.78 \pm 0.12$.

The inclusive hadron angular distributions discussed above are in excellent agreement with the jet model. These results strongly support the spin-$\frac{1}{2}$ parton picture of hadron production in e^+e^- annihilation.

VIII. CONCLUSIONS

Hadron production by e^+e^- annihilation has proved to be an extremely rich and interesting field of study. In this talk I have concentrated on results from experiments performed at energies away from the narrow resonances by the SLAC/LBL collaboration at SPEAR over the past two years. Some of the major results of these experiments may be summarized as follows:

1. In the SPEAR energy range, $2.4 \text{ GeV} \lesssim E_{c.m.} \lesssim 8 \text{ GeV}$, two extremely narrow resonances, $\psi(3095)$ and $\psi(3684)$, have been discovered. Aside from these resonances no additional narrow vector states have been found, and rather stringent limits have been set for the production of narrow resonances which couple directly to virtual photons with masses between 3.2 GeV and 7.6 GeV.

2. R exhibits three distinct regions over the SPEAR energy range. Below 3.5 GeV, R is approximately constant at a value near 2.5. Above 5 GeV, R is again nearly constant with a value about 5. Between these two scaling regions, there is a complicated transition region with several possible broad resonances.

3. The mean charged multiplicity and mean charged energy rise with increasing c.m. energy. The fraction of c.m. energy in charged particles falls from 0.6 to 0.5 over the SPEAR energy range.

4. Single particle inclusive spectra exhibit approximate Bjorken scaling for $x > 0.4$ and $3.0 \text{ GeV} \leq E_{c.m.} \leq 7.4 \text{ GeV}$. Above the 4 GeV region, scaling obtains for $x \gtrsim 0.2$. The inclusive spectra in the 4 GeV region seem to have a different shape from spectra at surrounding energies with an apparent excess of particles at intermediate values of x.

5. At 7.4 GeV, the inclusive angular distribution of hadrons was measured with the aid of polarized incident beams. Particles with low x are produced isotropically, while particles with $x > 0.2$ are produced predominantly through a transverse coupling to the virtual photon.

6. There is strong evidence for jet structure in hadron production by e^+e^- annihilation. The sphericity distribution is well represented by a simple limited transverse momentum jet model; a Lorentz-invariant phase space model disagrees with the data. The angular distribution of the jet axis indicates that the jets are mainly produced with net helicity one along the jet axis.

The next two talks will cover other work performed by the SLAC/LBL collaboration. The period of time since the Bonn Conference has been an incredibly rich one for physics, and exciting and rewarding for all of us who have participated in these experiments. We look forward to the next two years!

REFERENCES

1. K. Strauch, Proc. VI Int. Symposium on Electron and Photon Interactions at High Energies, Bonn, 1973 (North-Holland Publishing Co., Amsterdam, 1974), p. 1.
2. $\mu\pi$ Group: F. Ceradini et al., Phys. Letters 47B, 80 (1973).
   $\gamma\gamma$ Group: C. Bacci et al., Phys. Letters 44B, 533 (1973).
   Boson Group: B. Bartoli et al., Phys. Rev. D 6, 2374 (1972).
   BCF Group: M. Barnardini et al., Phys. Letters 51B, 200 (1974).
3. G. Cosme et al., Phys. Letters 40B, 685 (1972).
4. L. M. Kurdadze et al., Phys. Letters 42B, 515 (1972).
5. A. Litke et al., Phys. Rev. Letters 30, 1189 (1973); Ibid., 1349 (1973); G. Tarnopolsky et al., Phys. Rev. Letters 32, 432 (1974).
6. B. Richter, Invited talk at Conference on Lepton Induced Reactions, Irvine, California, December 1973.
7. B. Richter, Proc. XVII Int. Conf. on High Energy Physics, London, 1-10 July 1974 (Science Research Council, Rutherford Laboratory, 1974), p. IV-37.
8. J.-E. Augustin et al., Phys. Rev. Letters 33, 1406 (1974).
9. J. J. Aubert et al., Phys. Rev. Letters 33, 1404 (1974).
10. C. Bacci et al., Phys. Rev. Letters 33, 1408 (1974); Ibid., 1649 (1974).
11. W. Braunschweig et al., Phys. Letters 53B, 393 (1974).
12. G. S. Abrams et al., Phys. Rev. Letters 33, 1453 (1974).
13. J.-E. Augustin et al., Phys. Rev. Letters 34, 764 (1975).
14. Members of the SLAC/LBL Collaboration are: G. S. Abrams, J.-E. Augustin, A. M. Boyarski, M. Breidenbach, D. Briggs, F. Bulos, W. Chinowsky, G. J. Feldman, G. E. Fischer, C. E. Friedberg, D. Fryberger, G. Goldhaber, G. Hanson, D. L. Hartill, R. J. Hollebeek, B. Jean-Marie, A. D. Johnson, J. A. Kadyk, R. R. Larsen, A. M. Litke, D. Lüke, B. A. Lulu, V. Lüth, H. L. Lynch, D. Lyon, C. C. Morehouse, J. M. Paterson, M. L. Perl, F. M. Pierre, T. P. Pun, P. Rapidis, B. Richter, B. Sadoulet, R. F. Schwitters, W. Tanenbaum, G. H. Trilling, F. Vannucci, J. S. Whitaker, F. C. Winkelmann, J. E. Wiss, and J. E. Zipse.
15. J.-E. Augustin et al., Phys. Rev. Letters 34, 233 (1975).
16. A. M. Boyarski et al., Phys. Rev. Letters 34, 762 (1975).
17. H. Terazawa, Rev. Mod. Phys. 45, 615 (1973).
18. Radiative corrections were applied in the same manner as described in Ref. 13.
19. J. D. Bjorken, Proc. VI Int. Symposium on Electron and Photon Interactions at High Energies, Bonn, 1973 (North-Holland Publishing Co., Amsterdam, 1974), p. 25.
20. J. D. Bjorken, Phys. Rev. 179, 1547 (1969).
21. Y. S. Tsai, SLAC Report No. SLAC-PUB-1623 (1975), submitted to Phys. Rev.
22. A. A. Sokolov and I. M. Ternov, Sov. Phys.-Dokl. 8, 1203 (1964).

23. V. N. Baier, Sov. Phys.-Usp. 14, 695 (1972).

24. J. G. Learned, L. K. Resvanis, and C. M. Spencer, U. of Wisconsin Preprint COO-476 (1975), submitted to Phys. Rev. Letters.

25. R. P. Feynman, Photon-Hadron Interactions (W. A. Benjamin, New York, 1972).

26. R. F. Schwitters et al., SLAC Report No. SLAC-PUB-1629 (1975), to be published in Phys. Rev. Letters.

27. J. D. Bjorken and S. J. Brodsky, Phys. Rev. D 1, 1416 (1970).

28. G. Hanson et al., SLAC Report No. SLAC-PUB-1655 (1975), submitted to Phys. Rev. Letters.

DISCUSSION

M. Tannenbaum, Rockefeller University: For the jet analysis, did you only use the charged particles?

R. Schwitters: Yes, only charged particles.

Tannenbaum: What did you do with the neutrals?

Schwitters: The only information we have on neutrals on gamma rays would be direction information. They are therefore ignored both in the analysis of the data and in the Monte Carlo calculations.

K. Lane, Cornell: What is the integrated area under the 4.4 GeV bump?

Schwitters: The 4.4 GeV bump is roughly 50 MeV wide and you can pick the height yourself--say 10 nb. Therefore the area is probably less than 500 nb-MeV. It is much smaller than the areas of the ψ and ψ'.

G. Barbiellini, Frascati: Could you tell us the limiting factors in reaching a possible accuracy of 5 - 10% in measurements of the total cross section around the 4.1 GeV region?

Schwitters: The principal factors limiting our precision in measurements of the total cross section are the stability of the luminosity monitors, reproducibility of the detector trigger and event selection, and counting statistics. Both the luminosity monitoring and hadron event detection are limited in precision to about ± 5% over periods of a few days or a few weeks. Counting rates in the 4 GeV region correspond to approximately 200 detected hadron events per calendar day. Since we usually accumulate at least 100 events at each energy setting in the coarse scan of the 4 GeV region, we are always in the situation where drifts in the detector may be significant and can lead to point-to-point systematic errors on the order of 5 to 10%.

J. Rosner, University of Minnesota: Have you made any study of the inclusive photon cross section in the 4.1 GeV region, particularly its variation with beam energy?

Schwitters: No.

P. Garbincius, MIT: I was wondering if you had a plot of the sphericity in the region of the 4.1 GeV enhancement. It would be interesting to see whether the p_t limited phase space model continues to work in this region, especially with respect to resonance production.

Schwitters: I don't have such a plot.

[Note: Much of the discussion of SPEAR and DORIS results occurred after all the individual papers had been presented. See the separate section of these Proceedings called "SPEAR-DORIS DISCUSSION" for a report of these discussions.]